

Optimization of the OPLS-AA Force Field for Long Hydrocarbons

Shirley W. I. Siu,[†] Kristyna Pluhackova, and Rainer A. Böckmann*

Computational Biology, Department of Biology, Universität Erlangen-Nürnberg, Erlangen, Germany

S Supporting Information

ABSTRACT: The all-atom optimized potentials for liquid simulations (OPLS-AA) force field is a popular force field for simulating biomolecules. However, the current OPLS parameters for hydrocarbons developed using short alkanes cannot reproduce the liquid properties of long alkanes in molecular dynamics simulations. Therefore, the extension of OPLS-AA to (phospho)lipid molecules required for the study of biological membranes was hampered in the past. Here, we optimized the OPLS-AA force field for both short and long hydrocarbons. Following the framework of the OPLS-AA parametrization, we refined the torsional parameters for hydrocarbons by fitting to the gas-phase *ab initio* energy profiles calculated at the accurate MP2/aug-cc-pVTZ theory level. Additionally, the depth of the Lennard-Jones potential for methylene hydrogen atoms was adjusted to reproduce the densities and the heats of vaporization of alkanes and alkenes of different lengths. Optimization of partial charges finally allowed to reproduce the gel-to-liquid-phase transition temperature for pentadecane and solvation free energies. It is shown that the optimized parameter set (L-OPLS) yields improved hydrocarbon diffusion coefficients, viscosities, and gauche–trans ratios. Moreover, its applicability for lipid bilayer simulations is shown for a GMO bilayer in its liquid-crystalline phase.

1. INTRODUCTION

The properties of alkanes are of interest for numerous chemical, physical, and biological processes, like the design of oleophobic surfaces,¹ the design of superconductors based on hydrocarbons,² or the study of artificial or biological membranes. For the latter, the lengths and degree of saturation of the hydrocarbon chains of the lipids determine, e.g., the membrane thickness or the phase at a given temperature, i.e., whether the membrane adopts a gel-like state, is in a ripple phase or the liquid crystalline state.

Organization and ordering as well as transport processes of hydrocarbons can be studied on the molecular level using atomistic molecular dynamics simulations. For this purpose, a number of different force fields were derived in the past which frequently focused on individual aspects of hydrocarbons, such as their transport characteristics, phase behavior, or energetics. These force fields undergo a continuous refinement as longer time scales become accessible due to the increasing computational power and the development of efficient algorithms as well as more experimental data become available.

First simulation studies of alkanes go back to the mid 1970s by Ryckaert and Bellemans who investigated relaxation and diffusion times developing a united-atom model.^{3,4} This was subsequently refined, e.g., within the framework of the optimized potentials for liquid simulations united-atom (OPLS-UA) model⁵ and the Berger force field popular in simulations of lipid bilayers.⁶ Further development included extensions by Toxvaerd and Ungerer et al. developing anisotropic intermolecular potential functions^{7,8} and by different other groups to all-atom models.^{9–11}

Based on the observation of too large density and heat of vaporization for pentadecane in the original OPLS-UA model,⁵ Berger et al. refined the Lennard-Jones (LJ) parameters and combined them with bonded parameters from the GROMOS87 force field in the Berger force field for lipids. In 2001,

the GROMOS united-atom model (45A3) was reparameterized¹² for aliphatic hydrocarbons. It yields excellent agreement for the liquid properties of both short- and long-chain hydrocarbons at standard temperature. Also, the all-atom OPLS (OPLS-AA) force field parametrization for organic liquids from Jorgensen's lab^{10,13} performs well for short-chain alkanes, while significant deviations for the heats of vaporization from experimental values were reported for *n*-alkanes exceeding six carbon atoms.¹⁴ Additionally, as shown below, the OPLS-AA force field for alkanes results in a liquid-to-gel-phase transition for pentadecane well above 300 K (experimental value 283.1 K),¹⁵ thus delimitating the applicability of OPLS-AA for simulations of long alkanes or for lipids. A reparameterization of OPLS-AA for linear and branched alkanes with up to 8 carbons by Chang and Sandler¹¹ displays a similarly shifted phase transition for long alkanes (own results, data not shown). A different OPLS-AA parametrization by Kahn and Bruice¹⁶ focused mainly on the reproduction of the physical properties of alcohols and polyketides, however yielding too low densities for long alkanes (own results, data not shown). Not least because of the above problems for long hydrocarbons, the popular OPLS-AA force field for proteins is frequently inconsistently combined with a united-atom representation for the lipids in studies on membrane proteins.

Here, we reparameterized the OPLS-AA force field for alkanes and alkenes with improved heats of vaporization, densities, and phase transition temperatures. Following the original parametrization, the LJ parameters were systematically varied to reproduce the densities and the heats of vaporization of both short- and long-chain hydrocarbons. Simultaneously, the dihedral potential parameters were optimized on *ab initio* data.

Received: December 19, 2011

Published: March 10, 2012

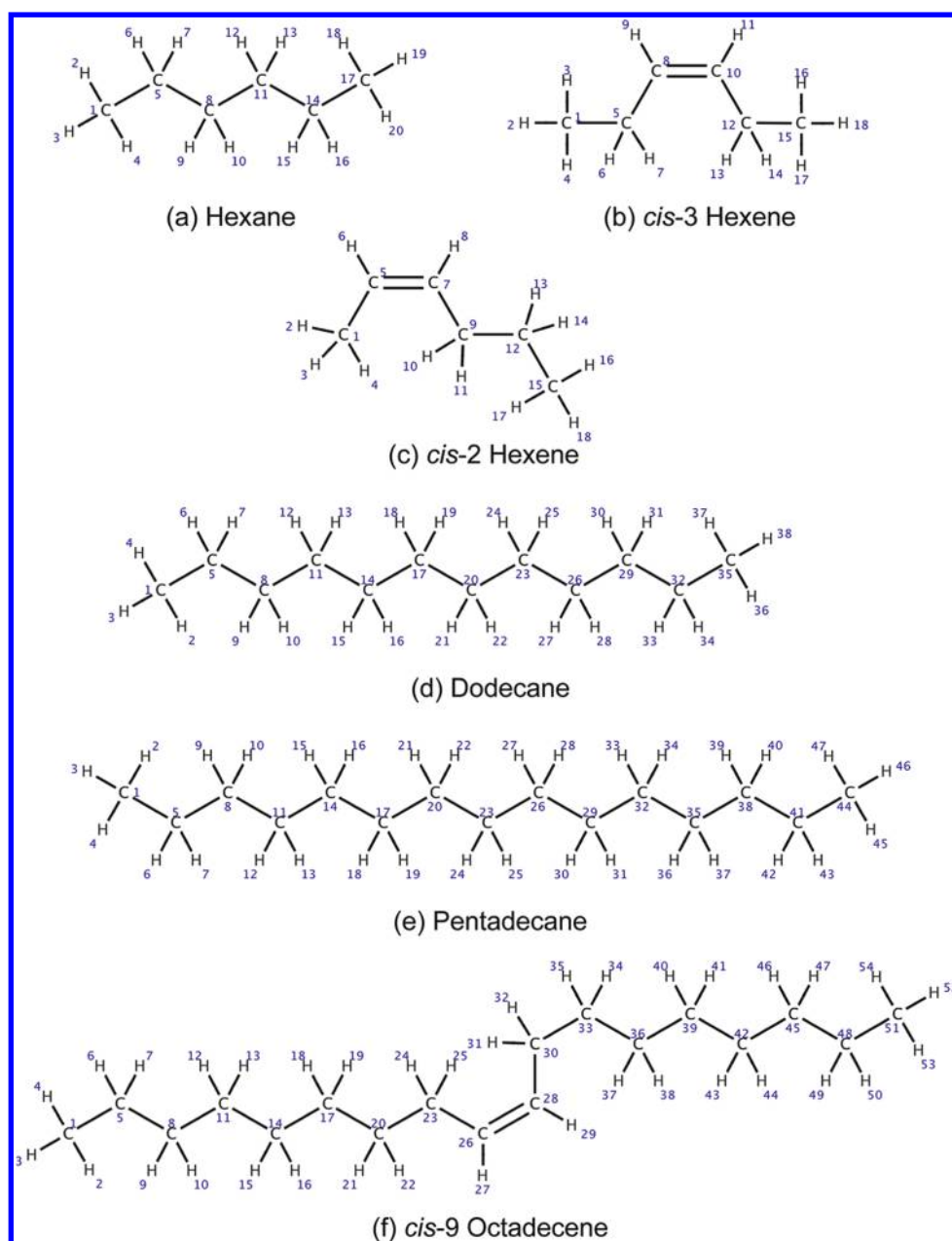


Figure 1. Hydrocarbon molecules used in this study. Atom numbers correspond to the numbering chosen in the Supporting Information topology files for simulation.

The correction of the torsional profiles improved the agreement of thermodynamic properties with experiments to such an extent that just a small adjustment of the depth (ϵ) of the LJ potential for methylene hydrogen atoms was required to obtain excellent agreement with experiment and also for long hydrocarbons, such as pentadecane. Additionally, and different from the standard protocol, hydrocarbon charges were adjusted to reproduce the phase transition temperature of pentadecane. The obtained optimized OPLS-AA parameter set for long hydrocarbons, termed L-OPLS, was validated on the diffusion of different alkanes, the viscosity, and the solvation free energy as well as on the distribution of *trans* and *gauche* states. We expect that the improved hydrocarbon parameters are in particular valuable for future force field development within the OPLS-AA framework for phospholipids. An initial test of L-

OPLS for a glycerol monooleate (GMO) bilayer correctly displayed the bilayer in its liquid crystalline state.

2. METHODS

Following the parametrization framework of the OPLS-AA force field,^{10,13} the OPLS-AA parameters for long hydrocarbons were optimized as follows: First, small molecules representing functional groups in hydrocarbons were chosen. Then for each small molecule, torsion scans using *ab initio* gas phase calculations were performed. The profile was fitted with the OPLS torsion function¹³ to obtain torsion parameters that minimized the relative energy differences between the *ab initio* profile, and the energy profile calculated from the force field. The van der Waals parameters, namely σ and ϵ in the LJ potential, were subsequently adjusted to reproduce the liquid densities and the heats of vaporization of hydrocarbons. In

addition, and different from the standard OPLS parametrization, the phase transition temperature for a long alkane (pentadecane) was fitted by fine adjustment of the atomic partial charges.

For saturated hydrocarbons, hexane was used for the torsional fit while *cis*-2 and *cis*-3 hexenes were used for unsaturated hydrocarbons. It was noted before for the OPLS force field that the deviation of the computed heats of vaporization for *n*-alkanes from the experimental values increases with increasing chain length *n*.¹⁴ Thus, instead of refitting the nonbonded parameters to small molecule properties, the parametrization was simultaneously performed on small and large alkanes (C_6H_{14} hexane, $C_{12}H_{26}$ dodecane, $C_{15}H_{32}$ pentadecane) and on alkenes (hexene C_6H_{12} , octadecene $C_{18}H_{36}$). The molecules used for the hydrocarbon parametrization are shown in Figure 1.

The final parameters were tested on a GMO bilayer in water. The system consisted of 200 GMO molecules, and the degree of hydration was 28 water molecules (of TIP3P-MOD water type) per GMO molecule. The simulations were started from a liquid crystalline phase of the bilayer and equilibrated for 100 ns at 310 K.

2.1. Ab initio Calculations. The *n*-alkane/alkene dihedral angle potentials are crucial in order to reproduce the (temperature-dependent) fraction of *trans* and *gauche* angles. Their distribution was also applied in the past to distinguish between L_α and L_β phases in phospholipid bilayer simulations.¹⁷

Dihedral torsion scans were performed every 2°, starting for every step from the reoptimized structure of the previous step. Thereby it is ensured that the calculation stays on the same potential energy surface. The internal coordinate corresponding to the torsion of interest was frozen while keeping all the other degrees of freedom flexible, thus allowing the molecule to relax. All geometries were obtained at the MP2/cc-pVDZ^{18,19} level of theory because the geometries of simple alkanes are known to be less sensitive to the size of the basis set than the energies itself. This approach proved to provide a good compromise between the computational cost and the quality of the geometry.²⁰ Energies of these geometries were then evaluated using a larger basis set, namely aug-cc-pVTZ.¹⁹

For the energy calculation, the torsion curve from MP2/aug-cc-pVTZ was compared to calculations using a higher level of theory, namely CCSD(T)/CBS. As shown in Figure 2, the results of both methods are comparable, thus ratifying our computational strategy. Instead of relying on relative energies

for *trans*/*gauche* states only,²⁰ detailed potential curves were computed.

Starting geometries were generated using MOLDEN²¹ and optimized to the minimum without any constraints using the same level of theory as for the other geometry optimizations. Møller–Plesset perturbation theory of the second order (MP2) calculations were performed using the TURBOMOLE 5.8 package,²² using standard self-consistent field (SCF) convergence criteria for evaluating the Hartree–Fock energy in every step of 10^{-7} Hartree and the standard total energy convergence criteria of 10^{-6} Hartree while applying stricter criteria for the maximum norm of the Cartesian gradient of 10^{-4} atomic units, ensuring better convergence to the energy minimum.

CCSD(T)/CBS energies were constructed according to the following equation:

$$E_{\text{CBS}}^{\text{CCSD(T)}} = E_{\text{CBS}}^{\text{MP2}} + (E^{\text{CCSD(T)}} - E^{\text{MP2}})_{\text{aTZ}} \quad (1)$$

where the MP2/CBS energy is obtained from the extrapolation of the MP2/aug-cc-pVDZ and MP2/aug-cc-pVTZ energies according to the scheme of Helgaker and co-workers.²³ The second term (difference between CCSD(T) and MP2 energies in a medium-sized basis set, namely, aug-cc-pVTZ) describes the higher order contributions to the correlation energy. It depends negligibly on the size of basis set.²⁴ All terms in eq 1 were obtained using the MOLPRO 2010.1 package of programs.²⁵

2.2. Fitting of Torsional Parameters. In OPLS, the Fourier function is used to describe the energetic contribution from a dihedral angle.¹³ This function can be converted into the form of the Ryckaert–Bellemans (RB) potential function,²⁶ and the coefficients of the Fourier function can be directly used in the RB function with some manipulations. The RB function is a sum of cosine terms with the dihedral angle ϕ :

$$V_{\text{RB}} = C_0 + C_1(\cos \phi) + C_2(\cos \phi)^2 + C_3(\cos \phi)^3$$

For efficiency, the RB function is used in the GROMACS simulation package,²⁷ which we used for all simulations reported below. Therefore, we directly fitted the torsion parameters to the RB function. Note that the RB parameters for hydrocarbons used in the Berger force field⁶ for lipid simulations included 1–4 interactions.³ Instead, within OPLS all 1–4 interactions are treated explicitly using scaled Coulomb and LJ potentials (scaling factor 0.5). For parametrization, the OPLS 1–4 scaling was applied.

The RB coefficients were obtained using a gradient-expansion algorithm to minimize the difference of the relative total potential energies calculated from the force field and from ab initio calculations.

2.3. Liquid- and Gas-Phase Simulations. Different from the original OPLS parametrization applying the Monte Carlo method (MC) to sample the configurational space, molecular dynamics simulations (MD) were used here.

All simulations were done with the GROMACS package, version 4.5.2.²⁷ The pure liquid simulations were performed by simulating 452 (hexane and hexene) or 216 (other molecules) randomly placed molecules equilibrated to the liquid density using the united-atom GROMOS S3a6 force field.²⁸ All-atom structures were created by adding aliphatic hydrogens, and the systems were equilibrated shortly for 300 ps with the original OPLS parameters to serve as starting structures for further

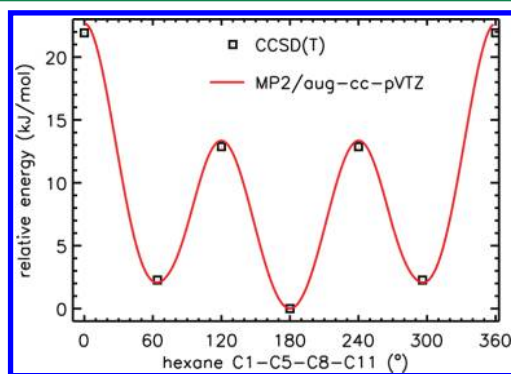


Figure 2. Comparison of the ab initio energy obtained by MP2/aug-cc-pVTZ to the accurate CCSD(T) method.

parametrization. The length of the cubic simulation boxes ranged from 4.3 to 4.8 nm.

Periodic boundary conditions were applied in liquid-phase simulations. Bonds and angles were kept flexible except for bonds involving hydrogens that were constrained using the LINCS algorithm,²⁹ allowing for an integration time step of 2 fs. The neighbor list was updated every 10 steps using a cutoff radius of 1.5 nm. Long range electrostatics was treated by the particle-mesh Ewald (PME) method with a grid spacing of 0.12 nm and cubic interpolation. The van der Waals interactions were treated using a switch function³⁰ between 1.1 to 1.3 nm to obtain smoothed forces at the cutoff boundaries. Beyond the cutoff, a correction was made to the energy of the LJ interactions and the system pressure.³¹ Simulations were carried out in the isothermal–isobaric ensemble (NPT). The temperature was coupled to a heat bath at 298.15 K using the velocity rescaling algorithm³² with a time constant of 0.1 ps. The system pressure was coupled isotropically by the Parrinello–Rahman barostat to 1 bar with a time constant of either 2.0 or 4.0 ps. Isothermal compressibilities of the system were taken directly from experiments. Data coordinates and energies were written out every 10 ps.

The gas phase of hydrocarbons was modeled by a single molecule in a large box. Both the translational and rotational center of mass motions of the molecule were removed every 10 steps. No cutoffs were used implying that all interactions were included in the energy calculations. The same temperature coupling method and hydrogen-bond constraints were applied as in the liquid simulations.

For force field comparisons, additional simulations were performed using the alkane parameters from the CHARMM36,^{20,33} the GROMOS G53a6,^{12,28} and the Berger force fields.⁶ The same simulation conditions were used for CHARMM and OPLS. For the united-atom models GROMOS and Berger, all bonds were kept constant. The long-range LJ correction was switched off for the GROMOS systems, as it was not used in the original parametrization.¹² The all-atom CHARMM and the united-atom GROMOS alkane parameters (named as the CHARMM36³³ and the G53a6_L³⁴ force fields, respectively) both yielded good agreement with experimental membrane properties in membrane simulation studies.^{33,34}

The heat of vaporization ΔH_{vap} was calculated as the difference in potential energy of a molecule in the gas phase $E(g)$ and the liquid phase $E(l)$:

$$\Delta H_{\text{vap}} = E(g) - E(l) + RT$$

where R is the gas constant and T the temperature.

Conformations of the alkyl chains were studied by investigating the gauche–trans population of the carbon–carbon torsions, i.e., $\phi(\text{CCCC})$ along the chain. The gauche and trans conformations were classified based on the torsional barriers at 120° and 240° between the two states. The gauche–trans fraction is calculated as the number of dihedral angles in gauche conformation divided by the total number of gauche/trans dihedrals.

Using the Einstein relation, the self-diffusion coefficient was calculated from the slope of the mean-square displacement (MSD) of the centers of mass averaged over the trajectories of each molecule:

$$D_s = \lim_{t \rightarrow \infty} \frac{\langle \Delta r(t)^2 \rangle}{6t}$$

where $\Delta r(t)$ is the distance that the molecule traveled in time t .

According to Yeh and Hummer,³⁵ a D_s obtained from simulations under periodic boundary conditions is system size dependent. Molecular diffusion in small to moderate sized systems is reduced due to long-range interactions between periodic images. Since the lengths of our simulation boxes ranged from 4.5 to 4.8 nm, a finite size effect is likely to be observed. A correction to D_s , D_s^{corr} , can be obtained by a straight-line fit to the self-diffusion coefficients as a function of the inverse box length and extrapolation to the infinite system limit. For hexane and pentadecane, 8- and 64-fold larger systems were studied to estimate the corrected diffusion coefficients.

Another transport coefficient, the shear viscosity, was calculated by the integration of the off-diagonal elements of the pressure tensor autocorrelation function from a NVT simulation (the Green–Kubo relation). Reported values are averages of the running integral in the plateau region, and standard errors were estimated from viscosities calculated independently from three pressure elements.

2.4. Hydration Free Energies. Free energies of hydration of selected alkanes/alkenes were computed from simulations by decoupling the solute molecule from the solvent separately for the electrostatic and the LJ interactions. The degree of coupling is parametrized by λ in the Hamiltonian ($\lambda = 1$ for the fully coupled state, $\lambda = 0$ for the decoupled state). An equidistant spacing for λ of 0.05 was chosen. Soft-core potentials as implemented in GROMACS with $\alpha = 0.5$ and $\sigma = 0.3$ were used with a soft-core power of 1. Free energy differences were extracted from the Bennett acceptance ratio between the n and $n + 1$ neighboring intermediate states. Each state was equilibrated for 0.5 ns, followed by 2 ns of data collection. Hydration free energies were determined for four different water models, the SPC/E,³⁶ the TIP3P,³⁷ the TIP3P-MOD,³⁸ and the TIP4P.³⁷

3. RESULTS OF PARAMETRIZATION

The OPLS parameters for hydrocarbons were taken from Price et al.,¹⁰ which contained a refinement of the alkane torsional parameters for OPLS-AA.¹³ The OPLS atom types, as shown in Table 1, were assigned to the hydrocarbon molecules. We

Table 1. OPLS Atom Types Used for Hydrocarbons

atom type	description	OPLS atom name(s) in GROMACS topologies
CT	alkane carbon	opls_135 (CH3), opls_136 (CH2)
CM	double-bonded carbon	opls_142 (C=C)
HC	aliphatic hydrogen	opls_144 (HC=), opls_140 (CH2, CH3)

followed the parametrization procedure as outlined in the Methods Section, and the results of the parametrization are presented in the following sections.

3.1. Gas-Phase Torsion Angles. In the OPLS-AA force field, the same torsional parameters of CT–CT–CT–CT were used for both the torsions involving the terminal methyl ($\text{CH}_3\text{--CH}_2\text{--CH}_2\text{--CH}_2$) and the middle torsion ($\text{CH}_2\text{--CH}_2\text{--CH}_2\text{--CH}_2$) in hydrocarbons. This approach was tested by comparing the ab initio torsional profile for the torsion C1–C5–C8–C11 and the torsion C5–C8–C11–C14 in hexane. The two profiles coincide except for the transition barrier between the gauche and the trans state, which is lower in the

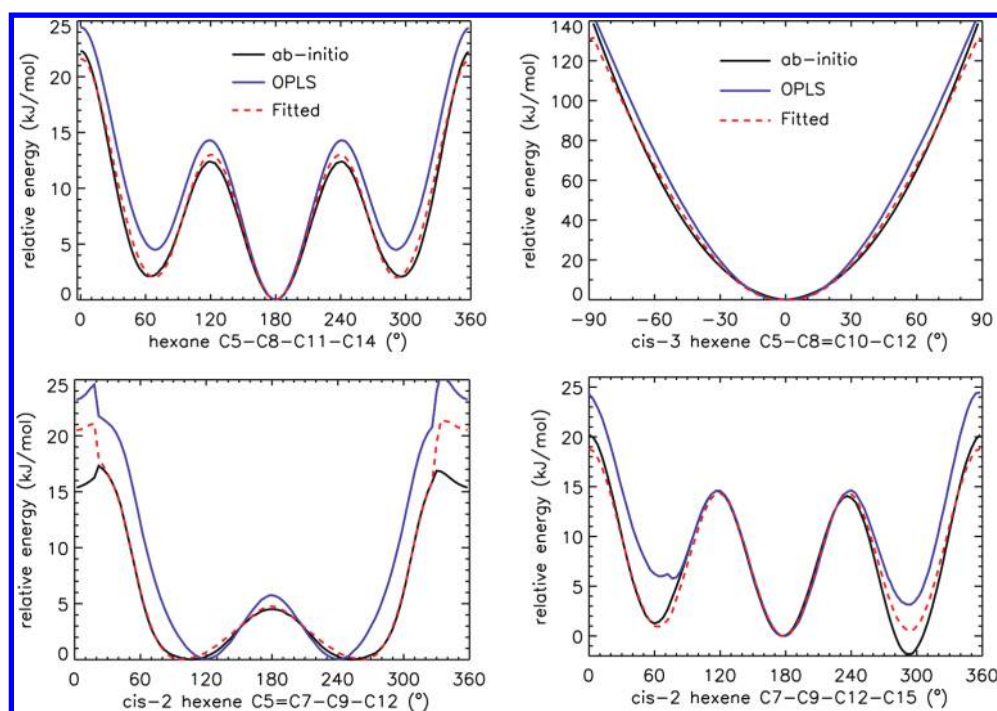


Figure 3. Relative energy profiles of the dihedral angle scan of hexane, *cis*-3 and *cis*-2 hexene.

Table 2. Optimized OPLS Parameters (L-OPLS) for Hydrocarbons^a

fitted torsion coefficients for the Ryckaert–Bellemans function (kJ/mol)						
OPLS torsion	molecule	ϕ	C_0	C_1	C_2	C_3
CT–CT–CT–CT	hexane	C5–C8–C11–C14	0.518787	–0.230192	0.896807	–1.49134
X–CM–CM–X	<i>cis</i> -3 hexene	C5–C8–C10–C12	51.25510	0.00000	–51.25510	0.00000
CM–CM–CT–CT	<i>cis</i> -2 hexene	C5–C7–C9–C12	–2.04906	1.03592	–1.34679	0.864221
CM–CT–CT–CT	<i>cis</i> -2 hexene	C7–C9–C12–C15	3.78614	0.106793	–0.562197	–1.48738
fitted torsion coefficients for Fourier dihedral (kJ/mol)						
OPLS torsion	molecule	ϕ	V_0	V_1	V_2	V_3
CT–CT–CT–CT	hexane	C5–C8–C11–C14	–0.305938	2.697394	–0.896807	0.74567
X–CM–CM–X	<i>cis</i> -3 hexene	C5–C8–C10–C12	0	0	51.2551	0
CM–CM–CT–CT	<i>cis</i> -2 hexene	C5–C7–C9–C12	–1.49571	–3.368171	1.34679	–0.4321105
CM–CT–CT–CT	<i>cis</i> -2 hexene	C7–C9–C12–C15	1.843356	2.017484	0.562197	0.74369
nonbonded parameters						
atom type	partial charge (e)		σ (nm)	ϵ (kJ/mol)		
CT _{CH₃}	–0.222		0.35*	0.276144*		
CT _{CH₂}	–0.148		0.35*	0.276144*		
CM _{CH}	–0.160		0.355*	0.317984*		
HC _{CH₃}	0.074		0.25*	0.125520*		
HC _{CH₂}	0.074		0.25*	0.110000		
HC _{CH}	0.160		0.242*	0.125520*		

^aDihedral parameters are given both for the RB potential and the Fourier functions (for the conversion see the Gromacs manual at www.gromacs.org). Values marked by asterisk were kept unmodified from the original OPLS-AA force field.

latter profile by only 1 kJ/mol. As this small difference is negligible, we used the same dihedral parameters for both torsions fitting the CH₂–CH₂–CH₂–CH₂ torsion.

The relative population of gauche–trans conformations of alkanes is mainly determined by the difference between the gauche and trans energy wells. It was reported in a previous hydrocarbon study using OPLS-AA that the average trans population of *n*-undecane is increased by about 9% with respect to experiment.¹⁴ This indicates that this force field over-

estimates the energetic difference between the hydrocarbon gauche and trans states.

A comparison of torsional profiles of hexane C5–C8–C11–C14 obtained from ab initio and force field calculations is shown in Figure 3. The ab initio profile (black line) was obtained from MP2/aug-cc-pVTZ single-point energy calculations of optimized structures at the MP2/cc-pVDZ level of theory (see Supporting Information for the ab initio torsion profiles). An average energy difference of 2.09 kJ/mol for the gauche–trans energy wells was obtained. In agreement with the

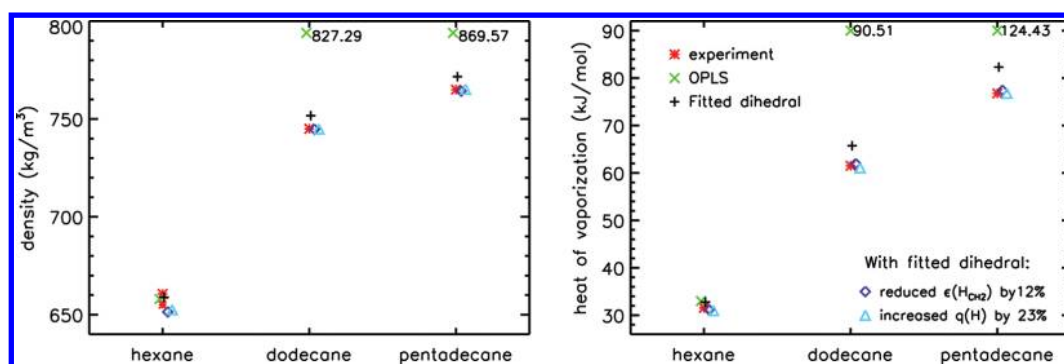


Figure 4. Densities and heats of vaporization of simulated hexane, dodecane, and pentadecane during parametrization. Experimental values are from refs 15, 39, and 40.

reported higher trans population in alkane simulations using OPLS-AA, the OPLS profile of the optimized single-point structures (blue line) yields an energy difference of 4.49 kJ/mol between the gauche–trans energy wells, twice as large as the corresponding ab initio value. To correct for this deviation, the torsion parameters of C5–C8–C11–C14 were refitted with the RB potential function. The fitted profile (dashed red) reproduces the ab initio profile with a rmsd of 0.46 kJ/mol.

Similarly, we fitted the three torsions of hexene: the torsion around the double bond in *cis*-3 hexene (C5–C8–C10–C12), the first neighboring torsion of the double bond in *cis*-2 hexene (C5–C7–C9–C12), and the second neighboring torsion (C7–C9–C12–C15). A comparison of the profiles is shown in Figure 3. The OPLS profile of the torsion around the double bond is fairly close to the ab initio profile, only a small refinement was required. However, the first neighboring torsion in the OPLS profile has a significantly narrower well at the two minima and an increased energy difference between the gauche and trans states.

Furthermore, the OPLS profile of the second neighboring torsion shows a large deviation of ~ 5 kJ/mol in relative energy for the two gauche states as compared to the ab initio profile. Fitting of the RB parameters allowed to reproduce the shape of the curve and the trans conformational energy. However, the difference between the two gauche states cannot be reproduced. The asymmetric relative energy at the two gauche states is likely caused by different interactions between the groups of atoms at the double bond and the methyl terminal at the two sides of the torsion: A distance of 1.1 nm between the centers of mass of the two groups for the g^+ state is measured, whereas a larger distance of 1.4 nm for the g^- state is found. However, the more favorable interaction at g^- could not be reproduced by simply fitting the dihedral, as this difference should be accounted for by nonbonded interactions instead of the torsion potential.

After fitting of the RB function on the three torsions separately, the rmsd of the fitted profiles from the respective ab initio profiles are 1.88 ($\pm 60^\circ$ around 0), 0.16, and 1.14 kJ/mol, respectively. The fitted RB coefficients for hydrocarbons are given in Table 2.

3.2. Thermodynamic Properties of Alkanes and Alkenes. Unlike in the original OPLS, we optimized the hydrocarbon nonbonded parameters by reproducing the densities and heats of vaporization of alkanes consisting of 6–15 carbon segments and of alkenes having 6–18 carbon segments. The need to use linear alkanes longer than six carbon segments for the hydrocarbon parametrization was previously

reported in different force field studies. For example, in the Berger lipid force field,⁶ pentadecane was used to guide the nonbonded parameter optimization. While the older GRO-MOS96 included alkanes of only up to six carbon segments for aliphatic carbon parametrization, the more recent version of the force field considered alkanes with chain lengths of up to 20 carbons.¹²

In this work, we included hexane, dodecane, and pentadecane for fitting the saturated hydrocarbon parameters. For unsaturated hydrocarbon parameters, we considered both hexene and octadecene. For each system and parameter set (see below), a simulation was run until equilibrium (monitored using both the density and the potential energy) was reached followed by a 10 ns production run used in data collection.

Figure 4 shows the evolution of the parameter optimization and a comparison of calculated thermodynamic properties to experiments. The OPLS force field reproduces the density and the heat of vaporization of hexane, but large deviations were obtained for long alkanes. MD simulations of dodecane and pentadecane using the OPLS force field moreover resulted in a phase transition after 2 ns (also when choosing the smaller cutoffs used in the parametrization of OPLS-AA). The hydrocarbon chains are seen to be densely packed and in high order. Interestingly, this phenomenon was not observed in an OPLS dodecane simulation using MC sampling.¹⁴ This probably points out problems in current MC schemes in sampling of cooperative processes, like phase transitions. Applying the fitted torsion parameters improved both thermodynamic properties significantly, resulting in an average error of 7% and 0.9% for the heats of vaporization and the densities of long alkanes, respectively. The larger deviations in the heats of vaporization suggest that a smaller ϵ value for either the hydrogen or the carbon atom is needed. A systematic test of different values of both σ and ϵ for hydrogen and carbon atoms on all three systems showed that a reduced ϵ of the methylene hydrogen atom (by 12.4%, i.e., from 0.125520 to 0.11 kJ/mol) yields the best agreement with experiment.

3.3. Gel-to-Liquid-Phase Transition Temperature. As shown above, the original OPLS dihedral parameters for alkanes promote phase transitions of long chain alkanes even at temperatures well above the experimental melting temperatures (T_m). Fitted dihedrals and additionally adjusted LJ parameters resulted in good agreement with the thermodynamic properties of alkanes at room temperature. Next, their effect on the phase transition temperature will be evaluated.

Reproducing the melting behavior of hydrocarbon parameters is particularly important, e.g., for simulating phospholipids

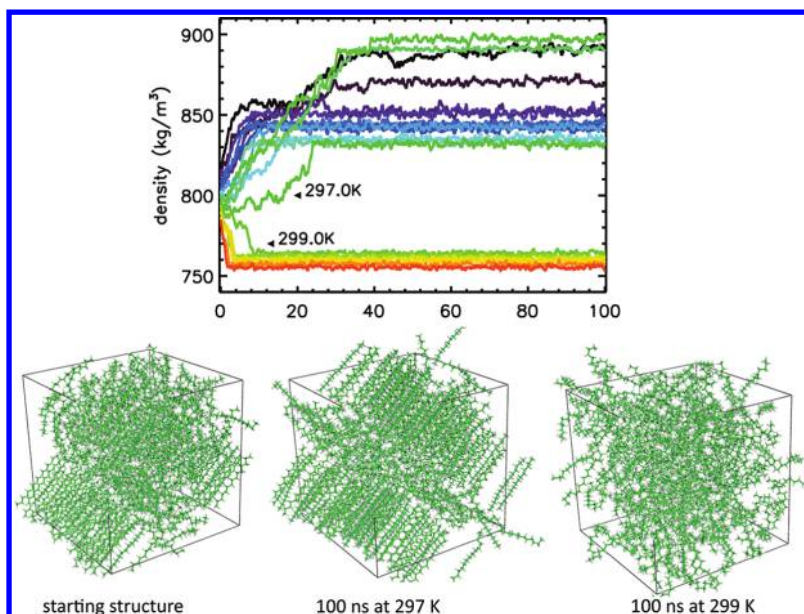


Figure 5. Density of the pentadecane temperature scan (with fitted dihedral and LJ parameters) performed for every 2 K from 273 to 321 K. The lower panel shows the starting half-gel structure and the final snapshots at 297 and 299 K. At temperatures below 297 K, all systems go to the gel phase, for $T > 299$ K, to the liquid phase.

with long hydrocarbon tails. An overestimated T_m for hydrocarbon tails might easily result in unrealistic phase transitions of modeled (bio)membranes. Therefore, in addition to the thermodynamic properties, fitting the hydrocarbon parameters to T_m will improve the robustness and applicability of the force field.

The transition temperature of the hydrocarbons studied here range from -141.11 °C (*cis*-2 hexene) to 9.95 °C (pentadecane).¹⁵ Since sampling at low temperatures is prohibitively slow, only the phase transition for pentadecane is used in the following for force field optimization. In order to accelerate the phase transition in particular close to T_m , a starting structure with mixed gel and liquid domains of pentadecane was used. This “half-gel” structure was obtained by simulating liquid pentadecane at 283 K until it reached a metastable state (after 50 ns) with roughly half-gel molecules in the box. The starting structure had a density of 820 kg/m³, about 7% increased in density as compared to the equilibrated liquid phase at 298.15 K. We determined the phase transition temperature of pentadecane using a series of simulations between 273 and 321 K ($\Delta T = 2$ K, 100 ns each), monitoring the density. Obtained profiles and selected snapshots of the simulations are shown in Figure 5. The estimated T_m for pentadecane (using the fitted parameters) was (298 ± 1) K, which is ~ 15 K above the experimental T_m .¹⁵ The differing densities for the gel phase were due to a varying number of molecules in a fluid-like state between layered gel-like structures (compare snapshots).

Averaged densities over the last 50 ns are shown in Figure 6 (black curve, using the default partial charge of $0.06e$ for aliphatic hydrogens, $q(H)$, in OPLS). Shifting of the phase transition temperature was achieved by modulating the charge of $q(H)$ and, correspondingly, changing the charge of the CH_2 and CH_3 atoms. A reduced $q(H)$ led to a rise in the T_m and an increased $q(H)$ lowered T_m . An increased $q(H)$ enlarges the charge–charge repulsion between molecules and increases the total potential of the system. This effectively reduces the amount of heat required to melt, thus the T_m is lowered.

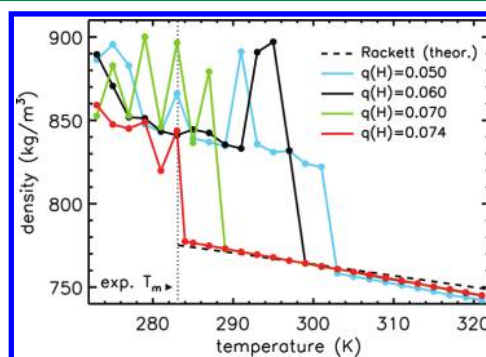


Figure 6. Temperature scan of pentadecane half-gel simulations applying different partial charges for the aliphatic hydrogen atom. The experimental T_m is 283.15 K.¹⁵ Each point refers to the average density over the last 50 ns of a 100 ns simulation at the respective temperature. The theoretical density curve of pentadecane above T_m is calculated from the modified Rackett equation $\text{density} = AB^{(1-T/T_c)^n}$, where $A = 0.24137$, $B = 0.25375$, $n = 0.31579$, $T_c = 706.80$ K, and T the target temperature.³⁹ $q(H)$ is given in units of the elementary charge e .

Different modulations of the charge distribution were tested, and the best agreement to the experimental T_m was obtained for $q(H) = 0.074e$, which amounts to a 23% increase in the hydrogen atom charge with respect to the default OPLS value. Recalculation of the densities and heats of vaporization for hexane, dodecane, and pentadecane showed that the new charge distribution has a vanishing effect on the fluid density at 298.15 K ($\leq 0.2\%$) and decreased the heat of vaporization by 0.5% (hexadecane), 1.4% (dodecane), and 0.8% (pentadecane) (see Figure 4).

Since the melting temperatures for alkenes under study are too low for systematic simulation studies addressing the phase transition temperature (hexene, $T_m = 132.04$ K; *cis*-9 octadecene, $T_m = 242.65$ K), the charge of the atoms composing the double bond was changed based on the free

Table 3. Densities (ρ in kg/m³) and Heats of Vaporization (ΔH_{vap} in kJ/mol) of Alkanes and Alkenes Using The OPLS Parameters and the Optimized Parameters Derived in This Study (L-OPLS)^a

	$E(g)$	$E(l)$	ΔH_{vap} (kJ/mol)	density (kg/m ³)
Hexane				
OPLS	65.07 ± 0.28	34.55 ± 0.03	33.00 ± 0.28	658.01 ± 0.32
L-OPLS	68.18 ± 0.27	39.67 ± 0.01	30.98 ± 0.27	652.50 ± 0.17
expt.			31.56 ^b	656 ^d , 660.6 ^b
Octane				
OPLS	85.83 ± 0.30	44.82 ± 0.03	43.49 ± 0.30	704.77 ± 0.31
L-OPLS	89.95 ± 0.17	51.29 ± 0.03	41.15 ± 0.18	698.45 ± 0.15
expt.			41.49 ^b	698.6 ^b
Decane				
OPLS	107.90 ± 0.46	54.42 ± 0.11	55.96 ± 0.47	735.91 ± 0.40
L-OPLS	111.86 ± 0.24	63.01 ± 0.03	51.33 ± 0.25	726.10 ± 0.16
expt.			51.42 ^b	726.6 ^b
Dodecane				
OPLS	129.86 ± 0.53	39.03 ± 0.11	93.31 ± 0.54	838.45 ± 0.39
L-OPLS	133.31 ± 0.21	74.73 ± 0.03	61.07 ± 0.22	744.89 ± 0.16
expt.			61.52 ^b	745.0 ^d
Pentadecane				
OPLS	164.58 ± 0.46	42.61 ± 0.12	124.45 ± 0.48	871.09 ± 0.29
L-OPLS	166.47 ± 0.45	92.16 ± 0.06	76.79 ± 0.45	765.20 ± 0.15
expt.			76.77 ^b	765.0 ^d
cis-2 Hexene				
OPLS	51.05 ± 0.29	20.94 ± 0.03	32.59 ± 0.29	692.23 ± 0.38
L-OPLS	58.22 ± 0.46	28.72 ± 0.01	31.98 ± 0.46	680.49 ± 0.18
expt.			32.19 ^b	683.0 ^d
cis-9 Octadecene				
OPLS	179.62 ± 0.72	83.63 ± 0.13	98.47 ± 0.74	794.75 ± 0.24
L-OPLS	185.55 ± 0.67	99.71 ± 0.05	88.33 ± 0.67	788.37 ± 0.10
expt.			80.05 ^{theor.c}	788.7 ^c

^aError estimates were obtained by block averaging (5 blocks of each 2 ns length). ^bExperimental values are taken from Haynes.¹⁵ ^cExperimental values are taken from Yaws.⁴¹ ^dExperimental values are taken from Yaws.⁴⁰ Literature data derived from theoretical equations rather than directly from experiment are indicated with *theor.*

energy of solvation for *cis*-2 hexene (see also below). Namely the charge was increased from 0.115 to 0.160e.

Finally, the improved OPLS parameter set for hydrocarbons with fitted dihedrals, the thermodynamic properties, and the gel-to-liquid phase transition temperature for pentadecane are summarized in Table 2, named L-OPLS. The equilibrium thermodynamic properties of both alkanes and alkenes are listed in Table 3.

4. L-OPLS FORCE FIELD EVALUATION

In the following, the performance of the L-OPLS force field for hydrocarbons is evaluated for the chain conformation, the self-diffusion of molecules, the viscosity, and the solvation free energy as well as for a simple GMO lipid bilayer.

4.1. Chain Conformation. The chain conformation was investigated by analyzing the population of the gauche and trans states in hydrocarbons. Since experimental values for tridecanes are available in the literature, we simulated and analyzed liquid tridecane in addition to other hydrocarbons (100 ns simulation for each force field).

The gauche–trans fraction as a function of the dihedral angle along the carbon chain is shown for tridecane in Figure 7. The terminal torsions led to an increased population of the gauche state relative to the trans state in all force fields investigated, resulting in a “bend” end-methyl conformation. In contrast, the gauche–trans fraction in the interior of the chain is almost constant for all investigated force fields. Similar trends were

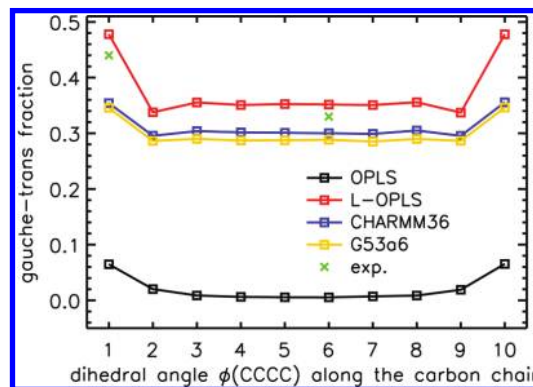


Figure 7. Gauche–trans fractions of tridecane as a function of dihedral angle along the carbon chain. Experimental values for the first and the sixth carbon torsions of tridecane are from Casal.⁴²

observed for hexane, dodecane, and pentadecane (data not shown). This is in accordance with the expectation that the chain terminals have a larger flexibility, while bond rotation is more restricted in the chain interior. Indeed, infrared spectroscopy experiments for specially deuterated tridecane showed a 33% increase in the population of gauche bonds for the terminal torsion as compared to the torsion in the middle of the chain.⁴² Comparison of the gauche–trans fractions for different force fields shows that L-OPLS overestimates the number of terminal gauche conformers by 8.6%, while both

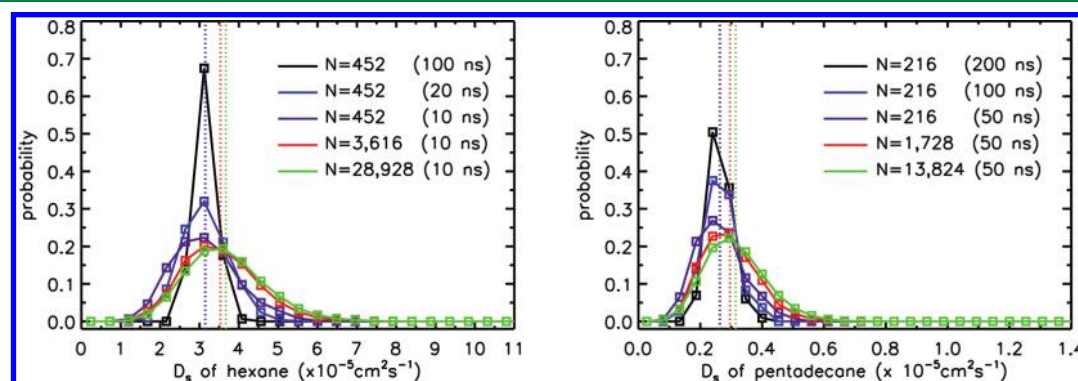
Table 4. Comparison of the Ratio of End Gauche (GT–), Double Gauche (–GG–), and Kink (–GTG–) Conformers per Molecule for Different Force Fields

	end gauche		double gauche		kink	
	tridecane	pentadecane	tridecane	pentadecane	tridecane	pentadecane
L-OPLS	0.70	0.70	0.63	0.81	0.64	0.85
CHARMM36	0.57	0.56	0.43	0.54	0.51	0.68
G53a6 _L	0.56	0.56	0.35	0.44	0.48	0.64
Berger		0.55		0.23		0.55
expt. ^a	0.68		0.64		0.77	

^aExperimental data are from Holler.⁴³**Table 5.** Comparison of Self-Diffusion Coefficients (D_s in $10^{-5} \text{ cm}^2 \text{ s}^{-1}$) of Liquid Hydrocarbons from Simulations Using Different Force Fields^a

	hexane	dodecane	pentadecane	cis-2 hexene	cis-9 octadecene
OPLS	2.992 ± 0.021	<0.01*	<0.01*	2.660 ± 0.005	0.095 ± 0.003
L-OPLS	3.151 ± 0.034	0.529 ± 0.013	0.264 ± 0.004	3.120 ± 0.017	0.160 ± 0.003
CHARMM36	3.050 ± 0.032		0.284 ± 0.006		
G53a6 _L	4.570 ± 0.062		0.673 ± 0.009		
Berger			0.957 ± 0.017		
expt.	4.210^b	0.871^c	0.461^c		

^a The diffusion coefficients D_s were obtained from the slope of the linear region of the MSDs, i.e., between 200–1000 ps for short chain hydrocarbons (hexane and hexene, simulation length of 10 ns) and between 2–5 ns for long chain hydrocarbons (simulation length of 100 ns). Standard errors were estimated by block averages³¹ (2 ns blocks for hexane and hexene, 20 ns blocks for the other molecules). ^bExperimental values are taken from McCall.⁴⁴ ^cExperimental values are taken from Tofts.⁴⁵ A finite-size correction to D_s is discussed in the text. Values marked by an asterisk denote systems in a gel phase.

**Figure 8.** Comparison of distributions of self-diffusion coefficients for systems with a varying numbering of molecules N (corresponding to box edge lengths between 4.6 and 18.55 nm) and different simulation lengths.

CHARMM36 and G53a6_L underestimate the gauche fraction by 19% and 21%, respectively.

Table 4 reports the number of different gauche conformers per molecule for both tridecane and pentadecane. The experimentally characterized conformations, the end gauche (GT–), the double gauche (–GG–), and the kink (–GTG–) conformations reveal the alkyl chain preference for nonlinear conformations in a liquid phase. The L-OPLS liquid simulation of tridecane predicts 0.70, 0.63, and 0.64 for the fractions of GT–, –GG–, and –GTG– conformations, yielding the best agreement to the experimental values of 0.68, 0.64, and 0.77 as compared to CHARMM36, G53a6_L, and Berger force fields, that underestimate the gauche population with an enhanced fraction of stretched conformations.

4.2. Diffusion Coefficients. Longer chains are slower in diffusion, and thus extended simulation lengths are required to reach linearity in the long-time regime of the MSD. As such, dodecane, pentadecane, and cis-9 octadecene simulations were extended to 100 ns.

The self-diffusion coefficients of hydrocarbons simulated with L-OPLS are compared to other force fields and experiments in Table 5 (see also Figure 8). L-OPLS shows a significant improvement in molecular diffusion over OPLS, but the calculated values exhibit a chain length-dependent deviation from experiment by 25%, 39%, and 43% for hexane, dodecane, and pentadecane, respectively. A deviation to a similar extent was observed for simulations using the all-atom CHARMM36 force field. In contrast, united-atom models (G53a6_L and Berger) overestimate the self-diffusivity of pentadecane by factors of 1.5 and 2.1, respectively.

For a more rigorous comparison of diffusion coefficients to experiments, a correction to account for the finite size effect is required.³⁵ Corrected diffusion coefficients D_s^{corr} for the L-OPLS force field were obtained by extrapolating to the infinite system size from simulations of different finite system sizes. The distribution of diffusion coefficients for different simulation lengths and different system sizes is shown in Figure 8. Increased simulation times narrow the distribution,

leaving the mean diffusion coefficient unchanged. In contrast, increased system sizes shift the distribution to larger diffusion coefficients. For L-OPLS, D_s^{corr} was exemplarily calculated for hexane ($3.865 \times 10^{-5} \text{ cm}^2 \text{ s}^{-1}$) and pentadecane ($0.329 \times 10^{-5} \text{ cm}^2 \text{ s}^{-1}$), yielding an improved agreement to experiment (deviations 8% and 29%, respectively). The correction increases the diffusion coefficient by 22% (hexane) and 24% (pentadecane), respectively.

4.3. Viscosities. The viscosities of hydrocarbons were computed for simulations using OPLS and L-OPLS and compared to experiments. As shown in Figure 9 and Table 6,

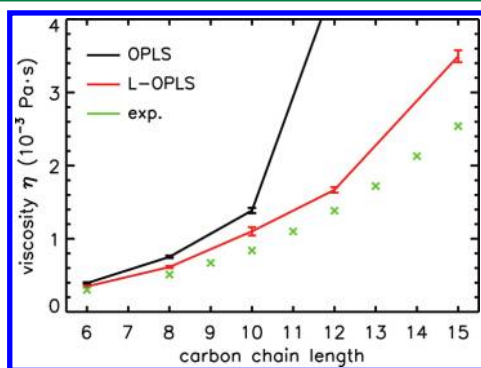


Figure 9. Liquid viscosities (η in $10^{-3} \text{ Pa}\cdot\text{s}$) of alkanes at 298.15 K.

OPLS results in increased deviations from experiments as compared to L-OPLS. Large viscosities obtained for dodecane and pentadecane using OPLS were caused by a transition into a gel-like phase for these systems. As for L-OPLS, the largest deviation from experiment is seen for pentadecane, yielding a 1.38 times larger viscosity. Similarly, improved results were obtained for the viscosities of alkenes (*cis*-2 hexene and *cis*-9 octadecene), being in good agreement with experiment. Finite-size effects were not considered, as they were shown before to not significantly influence the viscosity of fluids.³⁵

4.4. Solvation Free Energy. The influence of the adjusted van der Waals interactions and modified partial charges of hydrocarbons on solute–solvent systems was evaluated by determining the solvation free energy of different alkanes and of *cis*-2 hexene for different water models in frequent use (see Table 7).

The refined L-OPLS force field yields slightly increased solvation free energies for saturated hydrocarbons for a given water model type as compared to OPLS. The best performance of the water models was obtained for the TIP3P-MOD water³⁸ (maximum error is 6% and 20% for L-OPLS and OPLS force fields, respectively). This water model was developed to reproduce the free energy of solvation for methane and was shown to give excellent agreement also for the solvation free

energies of amino acid side chain analogs (discussed in detail by Shirts and Pande).⁴⁸ The original TIP3P model performed significantly better (maximum error of 14% and 8% for L-OPLS and OPLS, respectively) with respect to the SPC/E (errors between 30% and 50% for both force fields) and TIP4P (errors between 25% and 37%) models.

Using the original OPLS charges for the methylene hydrogen atom of *cis*-2 hexene, the solvation free energy for this molecule was $\approx 13\%$ larger than the experimental value for 1-hexene (using the TIP3P-MOD water model). The partial charges of the double bond carbon atoms were adjusted to reproduce the experimental solvation free energy (charge $-0.160e$).

4.5. GMO Bilayer Simulations. The effect of the improved description of hydrocarbon chains was evaluated on a GMO bilayer in water at full hydration (see Figure 10). Although the parameters for ester and glycerol groups remained unaltered, the effect of the new parameters on the bilayer structure is tremendous. While the original OPLS force field yields a gel-like structured bilayer with an area per lipid of 0.23 nm^2 at 310 K within 20 ns of simulation, the L-OPLS force field conserves the liquid crystalline phase of GMO for 100 ns of simulation time with an area per lipid of 0.32 nm^2 , close to the reported experimental area per lipid of 0.34 nm^2 ⁵¹ or 0.36 nm^2 .⁵² A similar area per lipid was obtained for extremely low hydration (2.5 water molecules per lipid) comparable to experiment (data not shown). Based on GMO simulations using the GROMACS force field yielding an area per lipid of 0.25 nm^2 , it was argued before that the experiments on GMO bilayers might reflect a stressed state of the membrane.⁵³ Our results indicate that the GROMACS force field probably underestimates the area per lipid for GMO due to gel phase formation.

5. DISCUSSION AND SUMMARY

An optimized OPLS-AA set of parameters for short- and long-chain alkanes and alkenes for use in all-atom molecular dynamics simulations is presented (L-OPLS). The parameters were refitted on ab initio dihedral potentials, on the densities and heats of vaporization of both short- and long-chain alkanes, and on the phase transition temperature of pentadecane. Apart from the dihedral parameters and hydrocarbon charges, the interaction strength of the methylene hydrogen atoms was modified. Tests of the L-OPLS parameters showed a significantly improved prediction of the gauche and trans fractions for alkanes as compared to the original OPLS-AA, CHARMM, or GROMOS force fields. Together with the decent agreement for the self-diffusion coefficients and the overall good prediction of viscosities for both saturated and unsaturated hydrocarbons, the optimized OPLS-AA parameter set provides a reliable force field for simulation studies of alkanes and alkenes.

Table 6. Liquid Viscosities (η in $10^{-3} \text{ Pa}\cdot\text{s}$) of Hydrocarbons for L-OPLS and OPLS at 298.15 K^a

	hexane	octane	decane	dodecane	pentadecane	<i>cis</i> -2 hexene	<i>cis</i> -9 octadecene
OPLS	0.393 ± 0.012	0.752 ± 0.016	1.386 ± 0.037	$>1400^*$	$>7000^*$	0.372 ± 0.004	7.739 ± 0.458
L-OPLS	0.348 ± 0.010	0.614 ± 0.015	1.102 ± 0.057	1.668 ± 0.038	3.496 ± 0.081	0.313 ± 0.013	4.320 ± 0.344
expt.	$0.3^b, 0.326^c$	0.51^c	0.84^c	$1.383^b, 1.508^c$	$2.54^c, 2.863^c$	$0.255^d, 0.2684^c$	4.31^e

^aDifferent lengths of NVT simulations were required to obtain reliable estimates for the viscosities: hexane 20 ns, octane 50 ns, decane and dodecane 100 ns, pentadecane 150 ns, hexene 50 ns, and octadecene 150 ns. ^bExperimental values are from Haynes.¹⁵ ^cExperimental values are from Tofts.⁴⁵ ^dExperimental values are from Yaws.⁴⁶ ^eExperimental values are from Yaws,⁴⁰ all at 298.15 K. For comparison, experimental values from Ivanciuc⁴⁷ obtained at 293.15 K are also listed. Values marked by asterisk denote systems in a gel phase.

Table 7. Comparison of the Free Energy of Solvations (ΔG_{sol} in kJ/mol) for Force Fields with Different Water Models^a

		SPC/E	TIP4P	TIP3P	TIP3P-MOD	expt. ^b
hexane	OPLS	13.59 ± 0.29	13.27 ± 0.24	11.56 ± 0.17	10.27 ± 0.14	10.67
	L-OPLS	14.42 ± 0.33	13.86 ± 0.20	12.06 ± 0.28	10.62 ± 0.14	
octane	OPLS	15.36 ± 0.21	15.09 ± 0.31	12.69 ± 0.18	11.10 ± 0.24	12.08
	L-OPLS	16.63 ± 0.25	16.40 ± 0.21	13.69 ± 0.24	11.65 ± 0.15	
pentadecane	OPLS	23.77 ± 0.29	21.57 ± 0.30	18.07 ± 0.21	13.81 ± 0.25	17.30 ^c
	L-OPLS	25.61 ± 0.25	23.78 ± 0.36	19.72 ± 0.24	16.34 ± 0.17	
<i>cis</i> -2 hexene	OPLS	11.90 ± 0.21	11.68 ± 0.09	9.67 ± 0.27	8.13 ± 0.15	7.24
	L-OPLS	10.93 ± 0.22	9.90 ± 0.17	8.45 ± 0.16	7.27 ± 0.14	

^aThe errors were determined by block averaging (5 blocks). ^bExperimental data were taken from Ben-Naim and Marcus⁴⁹ and Michielan et al.⁵⁰

^cTheor. value is derived from a fit to experimental results.

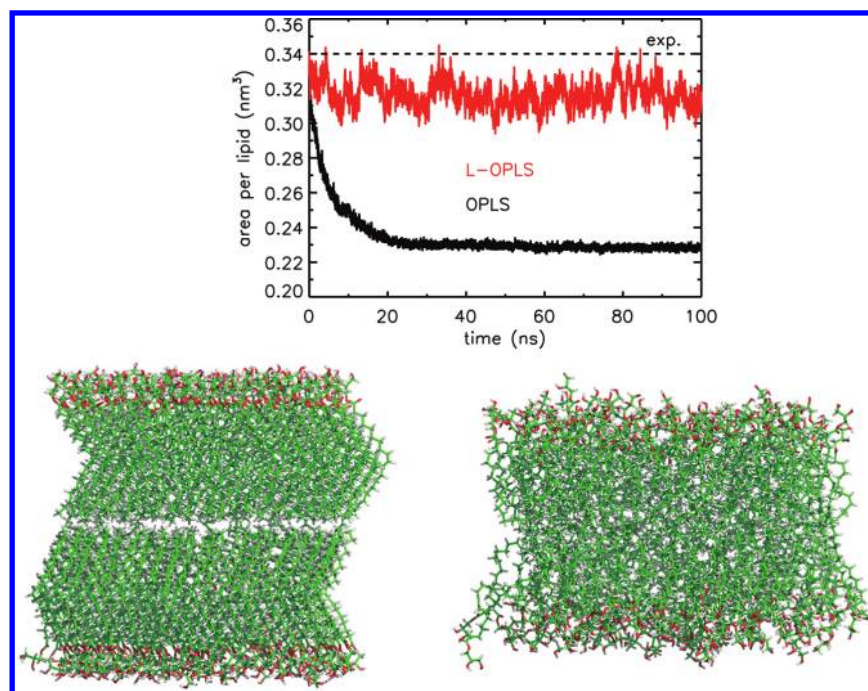


Figure 10. Comparison of GMO membrane simulations using the TIP3P-MOD water model at 310 K. The experimental area per lipid is taken from Briggs et al.⁵¹ Color codes: C (green), O (red), H (white), N (blue), and P (orange). Water molecules in the figures are omitted for clarity. The upper panel shows the area per lipid as a function of simulation time, and the lower panel simulation snapshots taken after 100 ns using the OPLS (left) and L-OPLS (right) force fields.

Both united-atom and the anisotropic united-atom models⁸ overestimate the diffusion of alkanes. In contrast, all-atom models underestimate the diffusion coefficients. The Marrink coarse-grained model⁵⁴ in turn overestimates the self-diffusion by roughly a factor of 4. This comparison suggests that further improvement in self-diffusion might require a fine coarse graining between united- and all-atom models. Results for the diffusion on short time scales as obtained from quasi-elastic neutron spectroscopy are probably very useful for a future refinement along this line.⁵⁵

With the significantly improved description of the phase transition temperature for pentadecane, L-OPLS is further anticipated to serve as a reliable basis, in particular for the modeling of phospholipids within the OPLS-AA framework. First results obtained for GMO bilayers correctly predicted the fluid crystalline phase, while usage of the original OPLS-AA parameters led to a phase transition to a gel-like state.

■ ASSOCIATED CONTENT

Supporting Information

Ab initio torsion profiles used in the fit of the dihedral parameters. Structures used for the analysis of torsion profiles and force field files for usage within the Gromacs simulation package are available on request and on www.biotechnik.nat.uni-erlangen.de/research/boeckmann. This material is available free of charge via the Internet at <http://pubs.acs.org/>.

■ AUTHOR INFORMATION

Corresponding Author

*E-mail: rainer.boeckmann@biologie.uni-erlangen.de. Telephone: ++49 +9131 85-25409.

Present Address

[†]University of Macau, Av. Padre Tomás Pereira Taipa, Macau, China.

Notes

The authors declare no competing financial interest.

■ ACKNOWLEDGMENTS

The authors thank Bert de Groot for stimulating discussions and the DFG for financial support (B02963/2-1). Computer time was provided by the Regionales Rechenzentrum Erlangen (RRZE).

■ REFERENCES

- (1) Tuteja, A.; Choi, W.; Ma, M.; Mabry, J. M.; Mazzella, S. A.; Rutledge, G. C.; McKinley, G. H.; Cohen, R. E. *Science* **2007**, *318*, 1618–1622.
- (2) Mitsuhashi, R.; Suzuki, Y.; Yamanari, Y.; Mitamura, H.; Kambe, T.; Ikeda, N.; Okamoto, H.; Fujiwara, A.; Yamaji, M.; Kawasaki, N.; Maniwa, Y.; Kubozono, Y. *Nature* **2010**, *464*, 76–79.
- (3) Ryckaert, J. P.; Bellemans, A. *Chem. Phys. Lett.* **1975**, *30*, 123–125.
- (4) Ryckaert, J. P.; Bellemans, A. *Faraday Discuss.* **1978**, *66*, 95–106.
- (5) Jorgensen, W. L.; Madura, J. D.; Swenson, C. J. *J. Am. Chem. Soc.* **1984**, *106*, 6638–6646.
- (6) Berger, O.; Edholm, O.; Jähnig, F. *Biophys. J.* **1997**, *72*, 2002–2013.
- (7) Toxvaerd, S. *J. Chem. Phys.* **1990**, *93*, 4290–4295.
- (8) Ungerer, P.; Beauvais, C.; Delhommelle, J.; Boutin, A.; Rousseau, B.; Fuchs, A. H. *J. Chem. Phys.* **2000**, *112*, 5499–5510.
- (9) Kaminski, G.; Duffy, E. M.; Matsui, T.; Jorgensen, W. L. *J. Phys. Chem.* **1994**, *98*, 13077–13082.
- (10) Price, M. L. P.; Ostrovsky, D.; Jorgensen, W. L. *J. Comput. Chem.* **2001**, *22*, 1340–1352.
- (11) Chang, J.; Sandler, S. I. *J. Chem. Phys.* **2004**, *121*, 7474–7483.
- (12) Schuler, L. D.; Daura, X.; van Gunsteren, W. F. *J. Comput. Chem.* **2001**, *22*, 1205–1218.
- (13) Jorgensen, W. L.; Maxwell, D. S.; Tirado-Rives, J. *J. Am. Chem. Soc.* **1996**, *118*, 11225–11236.
- (14) Thomas, L. L.; Christakis, T. J.; Jorgensen, W. L. *J. Phys. Chem. B* **2006**, *110*, 21198–21204.
- (15) Haynes, W. M. *CRC Handbook of Chemistry and Physics*, 91st ed.; Taylor and Francis Group, LLC: Boca Raton, FL, 2010–2011.
- (16) Kahn, K.; Bruice, T. C. *J. Comput. Chem.* **2002**, *23*, 977–996.
- (17) Egberts, E.; Marrink, S.-J.; Berendsen, H. J. C. *Eur. Biophys. J.* **1994**, *22*, 423–436.
- (18) Møller, C.; Plesset, M. S. *Phys. Rev.* **1934**, *46*, 618–622.
- (19) Kendall, R. A.; Dunning, T. H.; Harrison, R. J. *J. Chem. Phys.* **1992**, *96*, 6796–6806.
- (20) Klauda, J. B.; Brooks, B. R.; MacKerell, A. D., Jr.; Venable, R. M.; Pastor, R. W. *J. Phys. Chem. B* **2005**, *109*, 5300–5311.
- (21) Schaftenaar, G.; Noordik, J. H. *J. Comput.-Aided Mol. Design* **2000**, *14*, 123–134.
- (22) Ahlrichs, R.; Bär, M.; Häser, M.; Horn, H.; Kölmel, C. *Chem. Phys. Lett.* **1989**, *162*, 165.
- (23) Helgaker, T.; Jorgensen, P.; Olsen, J. *Molecular Electronic-Structure Theory*; John Wiley & Sons Ltd.: New York, 2002.
- (24) Jurečka, P.; Hobza, P. *Chem. Phys. Lett.* **2002**, *365*, 89–94.
- (25) Werner, H.-J.; Knowles, P. J.; Knizia, G.; Manby, F. R.; Schütz, M.; Celani, P.; Korona, T.; Lindh, R.; Mitrushenkov, A.; Rauhut, G.; Shamasundar, K. R.; Adler, T. B.; Amos, R. D.; Bernhardsson, A.; Berning, A.; Cooper, D. L.; Deegan, M. J. O.; Dobbyn, A. J.; Eckert, F.; Goll, E.; Hampel, C.; Hesselmann, A.; Hetzer, G.; Hrenar, T.; Jansen, G.; Köppl, C.; Liu, Y.; Lloyd, A. W.; Mata, R. A.; May, A. J.; McNicholas, S. J.; Meyer, W.; Mura, M. E.; Nicklass, A.; O'Neill, D. P.; Palmieri, P.; Pflüger, K.; Pitzer, R.; Reiher, M.; Shiozaki, T.; Stoll, H.; Stone, A. J.; Tarroni, R.; Thorsteinsson, T.; Wang, M.; Wolf, A. *MOLPRO, a package of ab initio programs*, version 2010.1; www.molpro.net, 2010.
- (26) Apol, E.; Apostolov, R.; Berendsen, H. J. C.; van Buuren, A.; Bjelkmar, P.; van Drunen, R.; Feenstra, A.; Groenhof, G.; Kasson, P.; Larsson, P.; Meulenhoff, P.; Murtola, T.; Pall, S.; Pronk, S.; Schulz, R.; Shirts, M.; Sijbers, A.; Tieleman, P.; Hess, B.; van der Spoel, D.; Lindahl, E. *GROMACS User Manual*, version 4.5.4; Royal Institute of Technology and Uppsala University: Stockholm and Uppsala, Sweden, 2010.
- (27) Hess, B.; Kutzner, C.; van der Spoel, D.; Lindahl, E. *J. Chem. Theory Comput.* **2008**, *4*, 435–447.
- (28) Oostenbrink, C.; Villa, A.; Mark, A. E.; van Gunsteren, W. F. *J. Comput. Chem.* **2004**, *25*, 1656–1676.
- (29) Hess, B.; Bekker, H.; Berendsen, H. J. C.; Fraaije, J. G. E. M. *J. Comput. Chem.* **1997**, *18*, 1463–1472.
- (30) van der Spoel, D.; van Maaren, P. J. *J. Chem. Theory Comput.* **2006**, *2*, 1–11.
- (31) Allen, M. P.; Tildesley, D. J. *Computer Simulations of Liquids*; Clarendon: Oxford, U.K., 1987.
- (32) Bussi, G.; Donadio, D.; Parrinello, M. *J. Chem. Phys.* **2007**, *126*, 014101.
- (33) Klauda, J. B.; Venable, R. M.; Freites, J. A.; O'Connor, J.; Tobias, D. J.; Mondragon-Ramirez, C.; Vorobyov, I.; MacKerell, A. D., Jr.; Pastor, R. W. *J. Phys. Chem. B* **2010**, *114*, 7830–7843.
- (34) Poger, D.; Mark, A. E. *J. Chem. Theory Comput.* **2010**, *6*, 325–336.
- (35) Yeh, I.-C.; Hummer, G. *J. Phys. Chem. B* **2004**, *108*, 15873–15879.
- (36) Berendsen, H. J. C.; Grigera, J. R.; Straatsma, T. P. *J. Phys. Chem.* **1987**, *91*, 6269–6271.
- (37) Jorgensen, W. L.; Chandrasekhar, J.; Madura, J. D.; Imprey, R. W.; Klein, M. L. *J. Chem. Phys.* **1983**, *79*, 926–935.
- (38) Sun, Y.; Kollman, P. A. *J. Comput. Chem.* **1995**, *16*, 1164–1169.
- (39) Yaws, C. L. *Chemical Properties Handbook*; McGraw-Hill: New York, 1999.
- (40) Yaws, C. L. *Yaws' Handbook of Physical Properties for Hydrocarbons and Chemicals*, 2008; http://www.knovel.com/web/portal/browse/display?_EXT_KNOVEL_DISPLAY_bookid=2147 (accessed February 26, 2012), .
- (41) Yaws, C. L. *Yaws' Thermophysical Properties of Chemicals and Hydrocarbons*, 2010; http://www.knovel.com/web/portal/browse/display?_EXT_KNOVEL_DISPLAY_bookid=2906 (accessed February 26, 2012), .
- (42) Casal, H. L.; Mantsch, H. H. *J. Mol. Struct.* **1989**, *192*, 41–45.
- (43) Holler, F.; Callis, J. B. *J. Phys. Chem.* **1989**, *93*, 2053–2058.
- (44) McCall, D. W.; Douglass, D. C.; Anderson, E. W. *Phys. Fluids* **1959**, *2*, 87–91.
- (45) Tofts, P. S.; Lloyd, D.; Clark, C. A.; Barker, G. J.; Parker, G. J. M.; McConville, P.; Baldock, C.; Pope, J. M. *Magn. Reson. Med.* **2000**, *43*, 368–374.
- (46) Yaws, C. L. *Yaws' Transport Properties of Chemicals and Hydrocarbons*, 2010; http://www.knovel.com/web/portal/browse/display?_EXT_KNOVEL_DISPLAY_bookid=2905 (accessed February 26, 2012), .
- (47) Ivanciuc, O.; Ivanciuc, T.; Filip, P. A.; Cabrol-Bass, D. *J. Chem. Inf. Comput. Sci.* **1999**, *39*, 515–524.
- (48) Shirts, M. R.; Pande, V. S. *J. Chem. Phys.* **2005**, *122*, 134508.
- (49) Ben-Naim, A.; Marcus, Y. *J. Chem. Phys.* **1984**, *81*, 2016–2027.
- (50) Michielan, L.; Bacilieri, M.; Kaseda, C.; Moro, S. *Bioorg. Med. Chem.* **2008**, *16*, 5733–5742.
- (51) Briggs, J.; Chung, H.; Caffrey, M. *J. Phys. II (France)* **1996**, *6*, 723–751.
- (52) Borne, J.; Nylander, T.; Khan, A. *Langmuir* **2000**, *16*, 10044–10054.
- (53) Marrink, S. J.; Mark, A. E. *J. Phys. Chem. B* **2001**, *105*, 6122–6127.
- (54) Marrink, S. J.; Risselada, H. J.; Yefimov, S.; Tieleman, D.; de Vries, A. H. *J. Phys. Chem. B* **2007**, *111*, 7812–7824.
- (55) Unruh, T.; Smuda, C.; Busch, S.; Neuhaus, J.; Petry, W. *J. Chem. Phys.* **2008**, *129*, 121106.